Available online at www.sciencedirect.com
ScienceDirect
Journal of Catalysis 251 (2007) 400–409
JOURNAL OF CATALYSIS
www.elsevier.com/locate/jcat

Electrochemical promotion of NO reduction by C_3H_6 on Rh catalyst-electrode films supported on YSZ and on dispersed Rh/YSZ catalysts

I. Constantinou [a], D. Archonta [a], S. Brosda [a], M. Lepage [b], Y. Sakamoto [c], C.G. Vayenas [a,*]

[a] *Department of Chemical Engineering, Caratheodory 1 St., University of Patras, GR-26504 Patras, Greece*
[b] *Toyota Motor Europe NV/SA, Technical Centre, Hoge Wei 33, B1930 Zaventem, Belgium*
[c] *Toyota Central R&D Laboratory Inc. Catalysis Div., Nagakute, Aichi 480-1192, Japan*

Received 13 April 2007; revised 19 June 2007; accepted 30 July 2007

Abstract

The selective catalytic reduction of NO by C_3H_6 in the presence of O_2 was investigated on porous polycrystalline Rh catalyst-electrode films deposited on YSZ (Y_2O_3-stabilized ZrO_2) and dispersed Rh/YSZ (0.5 wt%) catalysts. In the former case, it was found that the application of current or potential between the Rh catalyst-electrode and an Au counterelectrode enhanced the rate of NO reduction and CO_2 formation by factors of up to 55 and 200, respectively. These rate increases were strongly non-Faradaic with apparent Faradaic efficiencies, Λ, of up to 7000 for the formation of CO_2, demonstrating a significant effect of electrochemical promotion or non-Faradaic electrochemical modification of catalytic activity. A comparison of the activity between the electropromoted Rh paste catalyst and the dispersed Rh/YSZ catalyst shows that the TOFs on the dispersed Rh/YSZ catalyst fall between the corresponding TOFs on the unpromoted and electropromoted Rh catalyst-electrode film.
© 2007 Elsevier Inc. All rights reserved.

Keywords: Electrochemical promotion; Non-Faradaic electrochemical modification of catalytic activity, NO reduction; Rh catalyst-electrode; NO reduction by C_3H_6

1. Introduction

The application of small currents or potentials on porous catalyst films deposited on solid electrolytes leads to pronounced strongly non-Faradaic and reversible changes in catalytic activity and selectivity. This phenomenon is described as the electrochemical promotion of catalysis (EPOC) or electropromotion, or as non-Faradaic electrochemical modification of catalytic activity (NEMCA) [1–15].

Electrochemical promotion allows for the in situ control of catalyst activity and selectivity by controlling in situ the promoter coverage via potential application [1–17]. Work over the last 20 years has demonstrated that the phenomenon results from electrochemically controlled migration of promoting ionic species ($O^{\delta-}$, $Na^{\delta+}$) from the solid electrolyte support to the metal/gas exposed catalytic interface [9,13,14] and that classical promotion, electrochemical promotion, and metal–support interactions with O^{2-} conducting and mixed ionic–electronic supports are functionally identical and different only operationally [14–16].

The main parameters commonly used to describe the magnitude of electrochemical promotion are (i) the apparent Faradaic efficiency, Λ, defined as

$$\Lambda = \frac{\Delta r_{\text{catalytic}}}{I/2F}, \tag{1}$$

where $\Delta r_{\text{catalytic}}$ is the current or potential induced change in catalytic rate, I is the applied current, and F is the Faraday constant (96,480 C/mol), and (ii) the rate enhancement factor, ρ, defined as

$$\rho = r/r_0 = (r_0 + \Delta r_{\text{catalytic}})/r_0, \tag{2}$$

where r is the electropromoted catalytic rate and r_0 is the unpromoted (open circuit) catalytic rate.

* Corresponding author. Fax: +30 2610 997269
E-mail address: cat@chemeng.upatras.gr (C.G. Vayenas).

0021-9517/$ – see front matter © 2007 Elsevier Inc. All rights reserved.
doi:10.1016/j.jcat.2007.07.034

A reaction exhibits electrochemical promotion when $|\Lambda| > 0$, whereas electrocatalysis is limited to $|\Lambda| \leqslant 0$. When $\Lambda > 1$, the reaction is termed *electrophobic*; when $\Lambda < -1$, it is *electrophilic*. In the former case, the rate increases with catalyst potential, U, whereas in the latter case, the rate increases with decreasing catalyst potential. To date, Λ values up to 3×10^5 [1,13,14] and ρ values up to 1000 [14,18,19] have been reported for several catalytic systems.

An important question regarding the practical usefulness of electrochemical promotion is whether the turnover frequency (TOF) of a catalytic reaction on an electropromoted catalyst film (e.g., Pt or Rh on yttria-stabilized zirconia [YSZ]) can exceed the corresponding TOF for the same reaction on the same metal obtained with a fully dispersed nanocrystalline catalyst supported on the same support (e.g., YSZ). This is an important question from a practical standpoint as well as for understanding the extent to which thermal migration of promoting species from the support (e.g., $O^{\delta-}$) can match the electrochemically controlled promoting species migration, which is responsible for the NEMCA effect.

Reduction of pollutant emissions present in the exhaust of lean-burn and diesel engines has attracted great scientific interest in recent years [20–22]. One possible way to achieve high efficiency in this process is the selective catalytic reduction (SCR) of nitrogen oxides by hydrocarbons over noble metal catalysts. Rhodium is a quite selective catalyst for NO reduction but becomes unreactive under highly oxidizing (i.e., lean-burn) conditions due to surface Rh_2O_3 formation [23–26].

The main overall stoichiometric reactions occurring on the Rh catalyst-electrode are

$$C_3H_6 + 9NO \rightarrow 3CO_2 + (9/2)N_2 + 3H_2O, \quad (3)$$

$$C_3H_6 + 18NO \rightarrow 3CO_2 + 9N_2O + 3H_2O, \quad (4)$$

and

$$C_3H_6 + (9/2)O_2 \rightarrow 3CO_2 + 3H_2O. \quad (5)$$

In addition to these reactions and in high excess of oxygen in the gas phase, the oxidation of NO to NO_2 also occurs. The electrochemical promotion of Pt and Rh catalyst films for the reduction of NO by hydrocarbons, CO, and H_2 in absence of O_2 or with low O_2 concentrations has been studied in detail [4,10–12,14].

In the present study, to address the foregoing question regarding electrochemical promotion and metal–support interaction, the selective catalytic reduction of NO by propylene in the presence of a significant amount of oxygen was examined over Rh paste catalyst-electrodes supported on YSZ and compared with the performance of Rh catalysts finely dispersed on porous YSZ.

2. Experimental

2.1. Apparatus

The experimental apparatus and reactors used are presented schematically in Fig. 1 and have been described in detail previously [13,27–30]. The apparatus comprises three parts: the feed unit, the reactor, and the analysis unit. The feed unit uses certified gases of C_3H_6 (3000 ppm in He), NO (3000 ppm and 2% diluted in He), O_2 (1, 5, and 20% diluted in He), and ultrapure He (99.999%) for further dilution of the reaction mixture. The C_3H_6 and NO were provided by Messer Griesheim, and the O_2 and He were provided by Air Liquide. Gas flow rates were regulated by Brooks mass flow controllers connected to a four-channel Brose control box (model 5878). The total gas flow rate was 200 cm^3 (STP)/min.

The electrochemical promotion experiments were carried out in a "single pellet" reactor with a volume of ∼30 cm^3 [14] (Fig. 1a). Under the experimental conditions used in this study, this reactor behaved as a continuously stirred tank reactor (CSTR), as described in detail previously [13,14,31,32]. The reaction temperature was monitored via a thermocouple (type K) in contact with the sample.

The dispersed catalyst experiments were conducted in the reactor shown in Fig. 1b. This reactor behaved as a CSTR and had a volume of approximately 10 cm^3.

Gas analysis was performed using an online gas chromatograph (Hewlett Packard 5890 series II), a chemiluminescence analyzer (Eco Physics CLD 700 EL ht) for NO and NO_2, and an infrared analyzer (Rosemount Binos 100) for CO_2 for continuous analysis of the reactor feed and products. The gas chromatograph used a thermal conductivity detector (TCD) equipped with two columns, a Molecular Sieve 5A (for the detection of O_2, N_2, and CO) and a Porapak Q column (for the detection of C_3H_6, CO_2, and N_2O). Both TCD signals were integrated and recorded online by a Hewlett Packard integrator (model 3395). The chemiluminescence analyzer continuously detected the concentrations of NO and NO_2, and the infrared analyzer monitored the CO_2 concentration in the effluent stream. The signals of the two analyzer's were recorded on a three-channel pen recorder (Yokogawa Hokushin Electric, type LR 4120E). Currents or potentials were applied using an Amel Instruments model 533 potentiostat/galvanostat.

2.2. Catalyst preparation and characterization

2.2.1. Preparation of electropromoted films

The electropromoted Rh film catalysts were deposited on a disk of YSZ solid electrolyte (YSZ, 8 wt% Y_2O_3) and served as the working electrode of the electrochemical cell. The other two electrodes (reference and counter) were deposited on the other side of the disk (Fig. 1a). The YSZ disk was 1.9 cm in diameter and 2 mm thick. The geometric area of the working electrode was ∼2.1 cm^2, and those of the reference and counterelectrodes were ∼0.5 and ∼2.1 cm^2, respectively.

Gold counter and reference electrodes were deposited on the one side of the solid electrolyte plate via deposition of a thin paste layer (A1113 gold resinate; METALOR), followed by calcination first at 400 °C for 2 h (at a heating rate of 10 K/min) and then at 800 °C for 90 min (at the same heating rate). Blank experiments showed that the catalytic activity of the Au electrode was negligible compared with that of the Rh catalyst for the reactions under study.

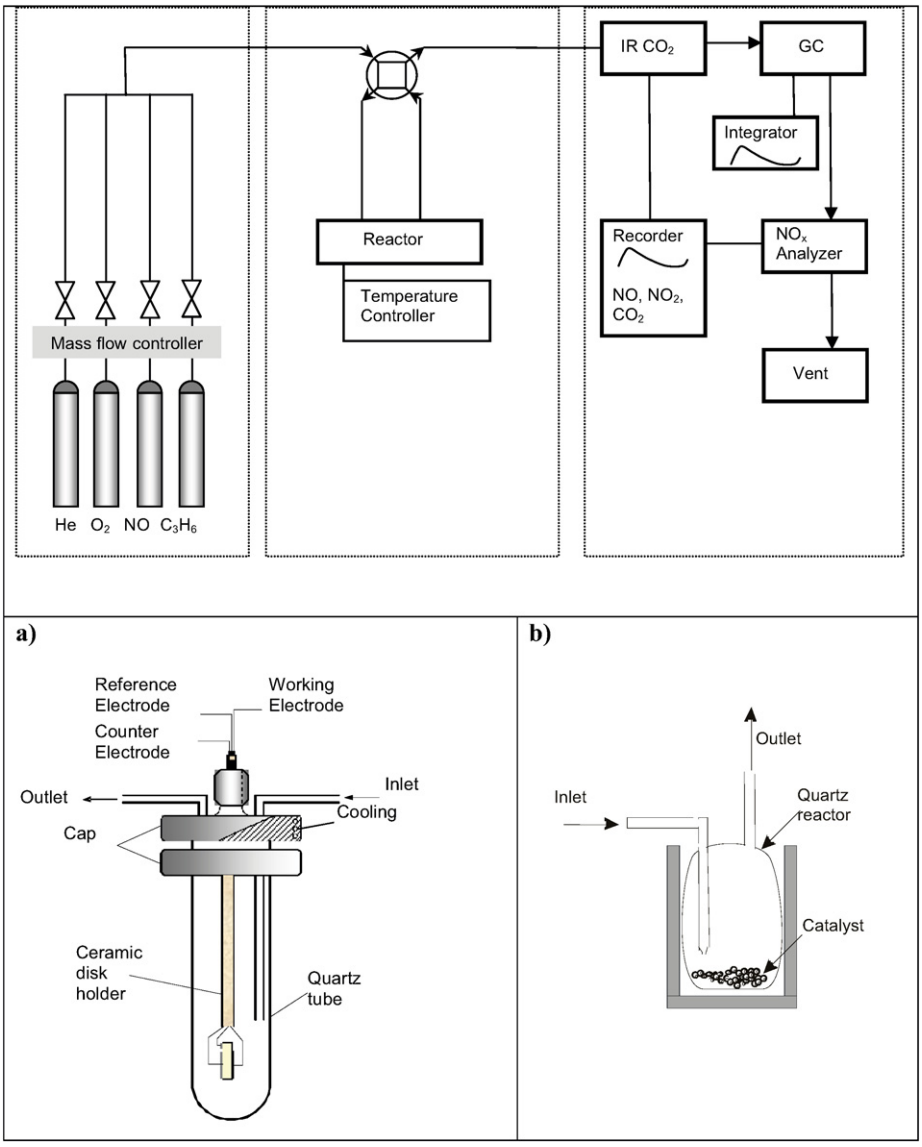

Fig. 1. Schematic of the experimental apparatus and of the two reactors used (a) for the electrochemical promotion of the Rh film catalysts and (b) for the dispersed catalyst experiments.

The Rh polycrystalline catalyst film (8826 rhodium resinate; METALOR) was deposited on the other side of the solid electrolyte, exactly opposite to the counterelectrode. This catalyst-electrode was calcined at 550 °C for 3 h with a heating rate of 3 K/min. The sample was reduced in situ in the reactor using 2% H_2 in He, with the temperature raised from 150 to 450 °C at a rate of 5 K/min, then remaining in the same reducing 2% H_2 mixture at 450 °C for 20 min. After reduction, the sample was cooled to the desired operating temperature (∼380 °C) at which the reactive NO, O_2, and C_3H_6 mixture was fed.

The surface area of the Rh catalyst films was estimated using the galvanostatic transient technique [13,14]. This technique involves first measuring the time, τ, required for the rate increase to reach 63% of its maximum steady-state value during anodic polarization, and then, assuming a 1:1 surface Rh:O ratio, estimating the reactive oxygen uptake of the Rh film and the active catalyst surface area, N_G, expressed in mol via [13,14]

$$N_G = I\tau/2F. \tag{6}$$

From Eq. (6), and taking the average of 10 galvanostatic and potentiostatic transient experiments at constant temperature, the active catalyst surface area, N_G, of the Rh film was estimated to be 4×10^{-7} mol Rh. Four such galvanostatic and potentiostatic transients are shown in Appendix A. The above N_G value was used to compute turnover frequencies (TOFs). Table 1 summarizes the properties of the Rh film catalyst-electrode.

2.2.2. Preparation of dispersed catalysts

The dispersed catalysts were prepared using a wet-impregnation method. Commercial YSZ (Tosoh 8Y-SZ) was used as the carrier, and a solution of $Rh(NO_3)_3 \cdot 2H_2O$ (Alpha Products) was used as the precursor. The YSZ support was impregnated with an aqueous solution of the metal precursor salt. Weighed

Table 1
Properties of the catalytic samples

Rh film deposited on YSZ disc		Dispersed Rh/YSZ catalyst	
		Metal dispersion	77%
Catalyst-electrode superficial area	~2.1 cm^2	Specific surface	345 m^2_{Rh}/g_{metal}
Counterelectrode superficial area	~2.1 cm^2	Mean size of metal particles	1.39 nm
Reference electrode superficial area	~0.5 cm^2	Total catalyst surface area	12 $m^2/g_{support}$
Actual surface Rh catalyst area expressed as surface metal mols, N_G	4×10^{-7} mol Rh	Total catalyst mass per catalytic testing	40 mg

amounts of $Rh(NO_3)_3 \cdot 2H_2O$ for the desired composition were dissolved in distilled water at 25 °C, followed by the addition of the desired amount of the carrier. After impregnation, the water was slowly evaporated at 80 °C under continuous stirring. The residue was dried at 120 °C for 24 h, and the resulting solid was ground and sieved. The powder catalyst was treated at 200 °C for 30 min under a flow of N_2, after which the flow was switched to 100% H_2 and the temperature was increased slowly to 300 °C, where the sample was held for 2 h. Finally, the sample was cooled to room temperature under a flow of N_2. The total metal loading was 0.5%, based on the total weight of the catalyst.

The total surface area of the support was estimated by the BET method, and the metal dispersion of the catalyst was obtained with H_2 chemisorption (Table 1). The adsorption isotherms in H_2 were determined by the volumetric technique using a modified Fisons Instruments Sorptomatic 1900 apparatus. The mass of the catalyst sample used for chemisorption was 1.0 mg. Measurements were performed at 25 °C in the pressure range of 0–75 Torr. Before each measurement, the catalyst was (i) pretreated by dynamic vacuum at 250 °C for 1 h, followed by (ii) reduction with 1 bar H_2 at 250 °C, and (iii) evacuation for 30 min at 250 °C, and (iv) finally cooled to room temperature under vacuum. Afterwards, the weakly adsorbed hydrogen was removed from the catalyst by evacuating the adsorption cell at room temperature for 10 min to a pressure of 10^{-6} Torr [33]. The total hydrogen uptake at monolayer coverage was obtained by extrapolation to the adsorption isotherm at zero pressure. The results are given in Table 1.

Before each experiment, an specific amount of fresh catalyst (ca. 40 mg, particle size of $0.18 < d < 0.25$ mm) was placed in the reactor and reduced at 300 °C for 30 min. Then the reactor was purged with He and the temperature was raised to 550 °C under He flow. The catalyst was maintained at that temperature for 1 h and then cooled under a flow of He to room temperature for measuring the metal dispersion (Table 1) or to the desired temperature for conducting the kinetic experiments. In the latter case, the feed was switched directly after the He purge to the reaction mixture, and light-off curves or steady-state measurements were obtained at given gas compositions in the temperature range of 100–550 °C.

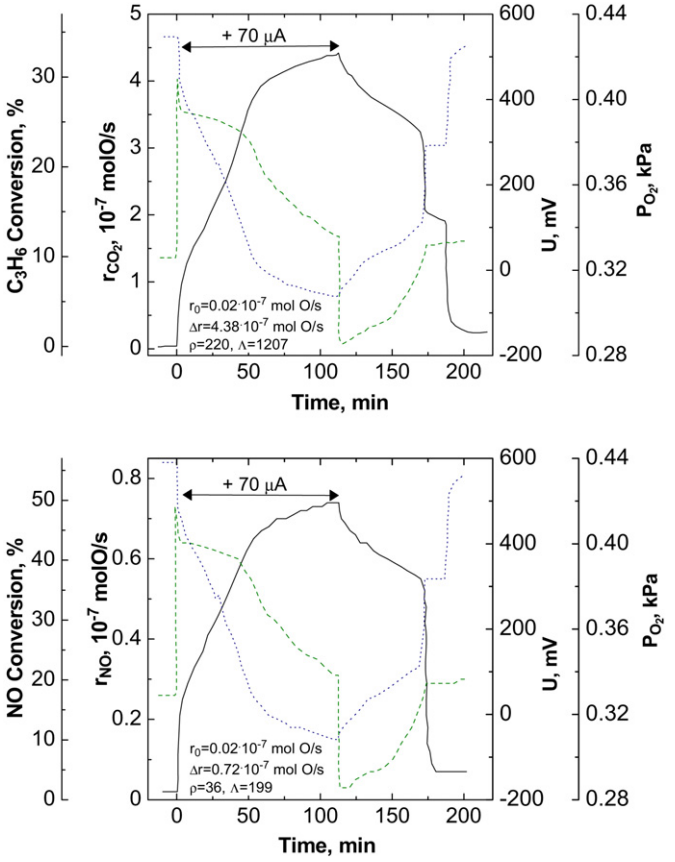

Fig. 2. Galvanostatic transient NEMCA experiment (application of +70 μA). Experimental conditions: $P_{NO} = P_{C_3H_6} = 0.1$ kPa, $P_{O_2} = 0.43$ kPa, $T = 370$ °C, $F_v = 200$ cm^3 (STP)/min; dotted line refers to the oxygen partial pressure and dashed line refers to the working electrode potential, U, during the transient. (Top) Conversion of propylene and rate of CO_2 formation. (Bottom) Conversion of NO and rate of NO consumption.

3. Results and discussion

3.1. Transient experiments

Fig. 2 shows a typical galvanostatic NEMCA experiment, demonstrating the transient effect of constant positive current application on the rates of CO_2 formation and NO reduction and on the catalyst potential U_{WR}. The experiment was carried out at fixed feed gas compositions of $P_{O_2} = 0.43$ kPa and $P_{C_3H_6} = P_{NO} = 0.1$ kPa at 370 °C. Initially, for $t < 0$, the circuit was open and the steady-state rates of C_3H_6 oxidation to CO_2 and of NO reduction to N_2 were equal to 0.02×10^{-7} and 0.02×10^{-7} mol O/s, respectively. At $t = 0$, a constant anodic current, ($I = 70$ μA) was applied between the catalyst and the counterelectrode. Oxygen ions, O^{2-}, were transferred from the YSZ support to the Rh catalyst-electrode at a rate, $I/2F$, equal to 0.36×10^{-9} mol O/s, where F is the Faraday constant. At the same time, the rate of C_3H_6 oxidation to CO_2 increased, and after 120 min, it approached a new steady state ($r = 4.4 \times 10^{-7}$ mol O/s). The increase in the catalytic rate Δr (=4.38×10^{-7} mol O/s) was 1200 times greater than that in the rate of ion transport, $I/2F$. This implies that each O^{2-} supplied to the rhodium catalyst surface caused on av-

erage 1200 chemisorbed O atoms to react with propylene and form CO_2 and H_2O. A 220-fold rate enhancement ($\rho = 220$) was observed, one of the highest ρ values ever observed in electrochemical promotion studies. The C_3H_6 conversion increased from 0.15 to 33%. At the same time, the rate of NO reduction increased from 0.02×10^{-7} to 0.74×10^{-7} mol O/s ($\Delta r = 0.72 \times 10^{-7}$ mol O/s). The latter corresponds to a 35-fold rate enhancement and a Λ value of 199. After current interruption, the catalytic rates of CO_2 formation and NO reduction returned to their initial open circuit value, demonstrating the reversibility of the phenomenon.

It also is interesting to examine the corresponding catalyst potential with respect to the reference electrode, U_{WR}, response in Fig. 2 (dashed line). When the current was first applied to the sample, the catalyst potential increased abruptly from 50 to 450 mV, indicating a change in the oxidation state of the catalyst. This behavior is quite common when the catalyst surface is initially oxidized (i.e., has a very high oxygen coverage, very likely forming an ordered monolayer surface Rh_2O_3 phase) [34] and the oxygen partial pressure in the feed is near the stoichiometrically required pressure for complete fuel combustion. Along with the potential U_{WR}, Fig. 2 also shows the actual oxygen partial pressure obtained from the oxygen mass balance (dotted line). It can be seen that after the application of current, the P_{O_2} dropped monotonously due to the increased propylene oxidation rate, and the potential exhibited a more complex transient, indicative of the reduction of the surface Rh_2O_3 phase. Note that the open-circuit potential was 50 mV before current application but dropped to −180 mV immediately after current interruption, indicating that the catalyst surface was indeed reduced to metallic Rh. It can be seen that under this new open-circuit potential value, the rates of CO_2 formation and NO consumption were very high. On current interruption, the gaseous oxygen oxidized the catalyst surface, as manifested by the gradual increase in catalyst potential back to its initial value (Fig. 2). This is in agreement with former studies of electropromoted Rh catalyst films [35,36] demonstrating that application of currents or potentials can have a significant (and reversible) effect on the stability limits of surface Rh oxide, thus significantly affecting the catalytic activity [14,37,38].

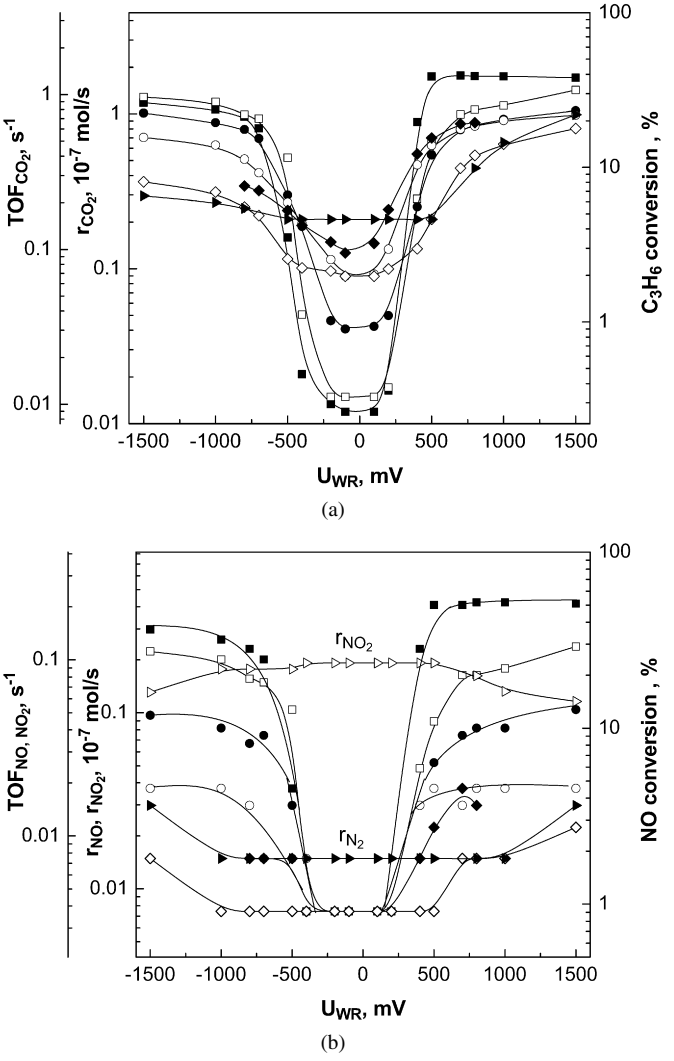

Fig. 3. Effect of catalyst potential on the rate and TOF of CO_2 production and on C_3H_6 conversion (a) and on the rates and TOFs of NO conversion to N_2 (b) at various P_{O_2} feed values. Experimental conditions: $P_{NO} = P_{C_3H_6} = 0.1$ kPa, $T = 370\,^{\circ}C$, $F_v = 200$ cm^3 (STP)/min. (■) $P_{O_2} = 0.5$ kPa, (□) $P_{O_2} = 0.67$ kPa, (●) $P_{O_2} = 0.88$ kPa, (○) $P_{O_2} = 1.26$ kPa, (◆) $P_{O_2} = 1.77$ kPa, (◇) $P_{O_2} = 2.5$ kPa, (►, ▷) $P_{O_2} = 4.8$ kPa for the rate of N_2 and NO_2 formation, respectively.

3.2. Effect of oxygen partial pressure

Fig. 3 shows the steady-state effect of oxygen inlet partial pressure and of catalyst potential on the rate and TOF of CO_2 formation, the conversion of C_3H_6 (Fig. 3a), and the rates and TOFs of N_2 and NO_2 formation and conversion of NO (Fig. 3b). The experiments were carried out at constant inlet partial pressures of NO and C_3H_6 equal to 0.1 kPa (1000 ppm) at 370 °C and at a constant flow rate of 200 cm^3 (STP)/min. The catalyst potential was varied from −1500 mV (cathodic polarization) to +1500 mV (anodic polarization). It can be seen that both reactions exhibited a pronounced *inverted volcano behavior* [14]; that is, the rates of C_3H_6 oxidation and NO reduction increased dramatically with both positive and negative potential. At higher oxygen inlet partial pressures, the electrochemical promotion was more pronounced at anodic polarization. This most likely is due to the weakening of the Rh=O bond via repulsive lateral interactions with co-adsorbed spillover $O^{\delta-}$ supplied electrochemically to the catalyst surface and the concomitant hindrance of the O poisoning of the catalyst surface [14]. At low oxygen inlet partial pressures, the C_3H_6 conversion increased from 0.2 to 40%. Under lean burn conditions (4.8% O_2), the effect was smaller, and rate increases on the order of 25% were observed. Under cathodic polarization (i.e., application of negative potentials), the rate increase most likely was due to the lower work function of the catalyst surface [14], which enhances NO adsorption and dissociation [34].

Fig. 3b presents the corresponding dependence of the NO consumption rate on the oxygen inlet partial pressure. As shown in the figure, the pronounced inverted-volcano behavior for NO reduction to N_2 was present for P_{O_2} values up to 2.5 kPa. In this range, the selectivity to N_2 was near 100%. When the oxygen

inlet partial pressure increased to 4.8 kPa, the effect diminished and; only under these conditions did significant NO_2 formation occur. During anodic and cathodic polarization in this high P_{O_2} range, the selectivity for N_2 formation increased slightly, but the rate of N_2 formation remained an order of magnitude smaller than the rate of NO_2 formation.

At low oxygen inlet partial pressures (and consequently low coverages), anodic polarization reduced the binding strength of oxygen on the catalyst surface, leading to a more active adsorbed oxygen species and enhancing the rate of propylene oxidation. The resulting decreased oxygen coverage liberated surface sites for NO chemisorption and reduction. The adsorbed hydrocarbon species generally reduced the coverage of adsorbed oxygen, also leading to higher NO reduction rates. At the highest inlet oxygen partial pressures, the oxygen coverage was high, the Rh active sites were occupied almost completely by oxygen, and surface Rh_2O_3 was formed [36]. This is the reason why at such high inlet oxygen pressures the conversions were low and the electrochemical promotion effect was lower as well, because anodic polarization of the Rh film was not sufficient to decompose the surface Rh_2O_3 [39].

3.3. Effect of hydrocarbon partial pressure

The effect of hydrocarbon partial pressure, $P_{C_3H_6}$, on the rates of formation of CO_2 and N_2 is shown in Figs. 4a and 4b. The inlet partial pressure of NO was kept constant at 0.1 kPa and that of oxygen was kept constant at 1.25 kPa. The experiments were performed at 370 °C and at a constant flow rate of 200 cm^3 (STP)/min. The C_3H_6 inlet partial pressure was varied from 150 ppm to 2000 ppm, and the applied potential was between −1500 and +1500 mV.

In general, increasing the propylene inlet partial pressure was found to increase significantly both the unpromoted and electropromoted rates of CO_2 formation (Fig. 4a) and the electropromoted rate of NO reduction to N_2 (Fig. 4b). At the highest propylene partial pressure ($P_{C_3H_6} = 2000$ ppm), the open circuit rate of NO consumption is significantly increased as well. As expected in view of Fig. 3, both anodic and cathodic polarization cause a significant increase in both catalytic rates (*inverted volcano behavior* [14]).

It is clear from Figs. 3 and 4 that the $P_{C_3H_6}/P_{O_2}$ ratio of the reaction mixture has a significant effect on the open-circuit catalytic and electropromoted rates. It is known [23] that NO dissociates only at reduced active Rh sites, producing adsorbed N and O atoms, and that a combination of two adsorbed N atoms leads to dinitrogen formation. Thus, high hydrocarbon partial pressures maintain the surface in a reduced state and decrease the surface coverage of O, accelerating the rate of NO dissociation and N_2 desorption, as has been observed experimentally.

These observations are summarized and quantified in the three-dimensional Figs. 5–7 which show the effect of catalyst potential and $P_{C_3H_6}/P_{O_2}$ ratio on the rates of CO_2 and N_2 formation (Fig. 5), the rate enhancement ratios ρ_{CO_2} and ρ_{N_2} (Fig. 6), and the corresponding Faradaic efficiency values Λ_{CO_2} and Λ_{N_2} (Fig. 7). As already noted, ρ_{N_2} reaches values on the order of 60 for high $P_{C_3H_6}/P_{O_2}$ ratios with corresponding Λ_{N_2}

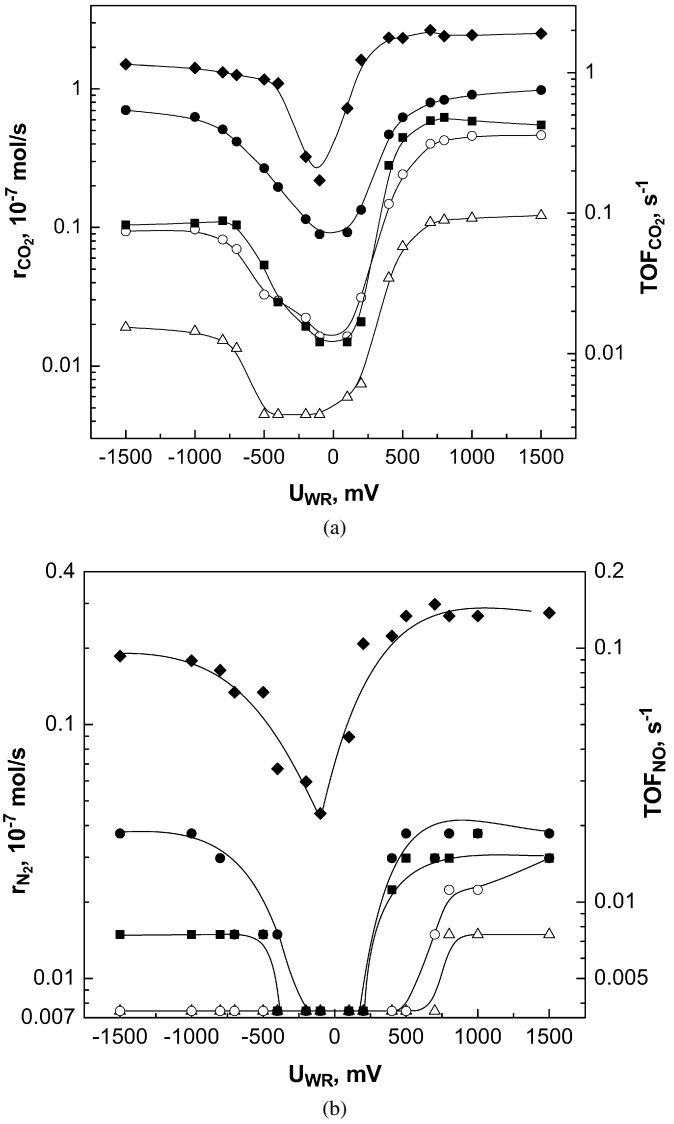

Fig. 4. Effect of catalyst potential and $P_{C_3H_6}$ on the rates and TOFs of CO_2 formation (a) and NO reduction (b). Experimental conditions: $P_{NO} = 0.1$ kPa, $P_{O_2} = 1.25$ kPa, $T = 370$ °C, $F_v = 200$ cm^3 (STP)/min. (△) $P_{C_3H_6} = 150$ ppm, (○) $P_{C_3H_6} = 500$ ppm, (■) $P_{C_3H_6} = 750$ ppm, (●) $P_{C_3H_6} = 1000$ ppm, (◆) $P_{C_3H_6} = 2000$ ppm.

values of up to 400, but the electropromotion effect gradually diminishes as the $P_{C_3H_6}/P_{O_2}$ ratio is decreased below 0.15 due to the formation of surface Rh_2O_3 [14].

The Faradaic efficiencies Λ_{CO_2} and Λ_{NO}, increased significantly with increasing $P_{C_3H_6}/P_{O_2}$. At the highest $P_{C_3H_6}/P_{O_2}$ ratio used, and for small overpotentials (<500 mV), the measured Faradaic efficiency values, Λ_{CO_2}, were as high as 7000. These Faradaic efficiencies are by an order of magnitude higher than those obtained at the lowest $P_{C_3H_6}/P_{O_2}$ ratio. Similar behavior was observed for NO reduction. The Faradaic efficiency, Λ_{NO}, for small overpotentials (<500 mV) varied from 50 at the lowest $P_{C_3H_6}/P_{O_2}$ ratio to 550 at the highest $P_{C_3H_6}/P_{O_2}$ ratio.

The measured Faradaic efficiency and rate enhancement ratio values were of comparable magnitude with those obtained recently on Ir [40] and Pt [41] catalysts for the SCR of NO.

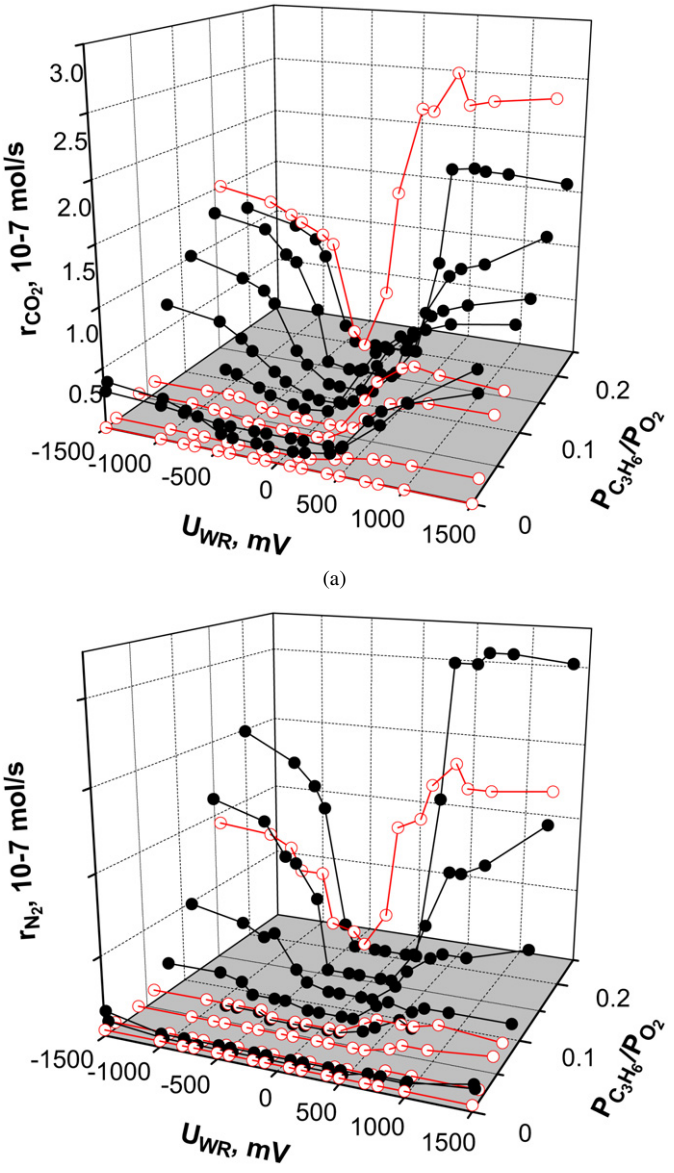

Fig. 5. Effect of catalyst potential and $P_{C_3H_6}/P_{O_2}$ feed ratio on the rates of (a) CO_2 formation and (b) N_2 formation as a function of catalyst potential for different propylene inlet partial pressures. Experimental conditions: $P_{NO} = 0.1$ kPa, $P_{O_2} = 1.25$ kPa, $T = 370\,^{\circ}C$, $F_v = 200$ cm^3 (STP)/min. Open symbols refer to constant oxygen inlet pressure of 1.25 kPa and filled symbols refer to constant propylene inlet partial pressure of 0.1 kPa.

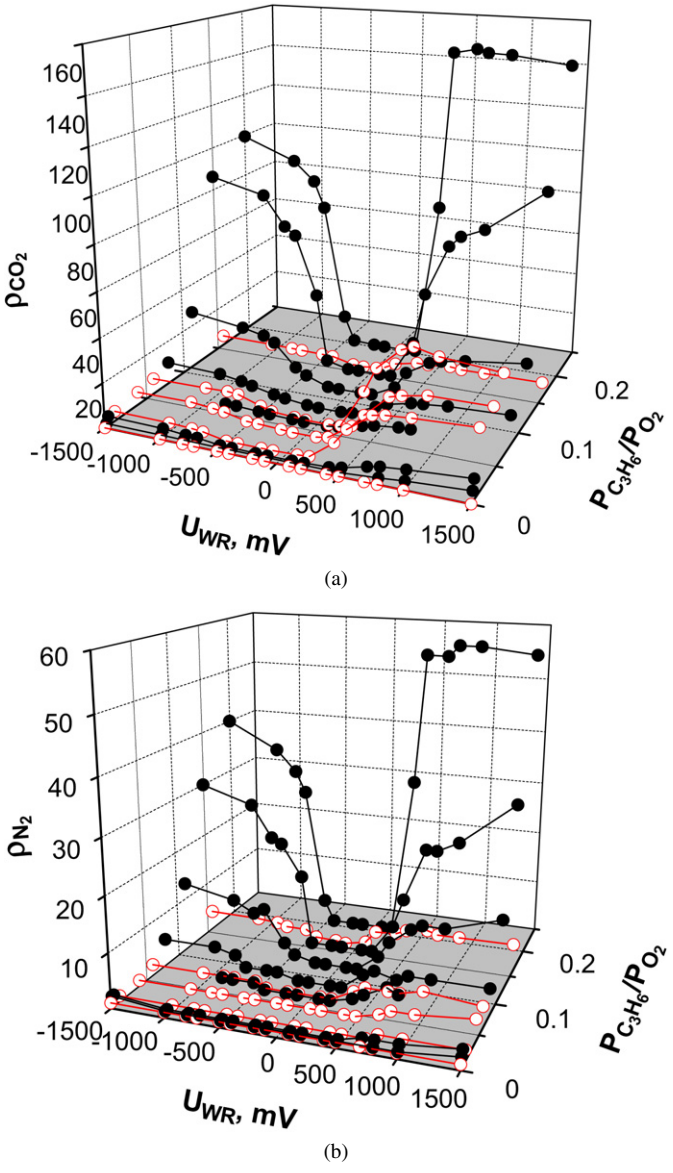

Fig. 6. Effect of catalyst potential and $P_{C_3H_6}/P_{O_2}$ feed ratio on the rate enhancement ratio of CO_2 (a) and N_2 (b) formation rate as a function of propylene to oxygen inlet partial pressures. Experimental conditions: $P_{NO} = 0.1$ kPa, $T = 370\,^{\circ}C$, $F_v = 200$ cm^3 (STP)/min. Open symbols refer to constant oxygen inlet pressure of 1.25 kPa and filled symbols refer to constant propylene inlet partial pressure of 0.1 kPa.

3.4. Comparison of electropromoted and dispersed catalysts

As discussed earlier, an important question regarding the practical usefulness of the electrochemical promotion effect for this and other catalytic systems is to what extent the TOFs on the electropromoted electrode surface can exceed the corresponding TOFs of fully dispersed commercial catalysts where the O^{2-} spillover mechanism is also operative [14]. Figs. 8 (TOFs for CO_2 formation) and 9 (TOFs for NO formation) present direct comparisons between electropromoted and dispersed Rh on YSZ catalysts. It can be seen that, in general, the TOF values of the dispersed catalysts fall between the TOFs on the promoted and unpromoted Rh paste catalyst-electrodes. This implies that the dispersed catalysts are, to some extent, partially promoted due to thermal migration of the promoting O^{2-} species from YSZ to the dispersed catalyst surface [14]. It should be noted that the TOFs compared in Figs. 8 and 9 were based on the number of surface Rh atoms, which did not change when surface Rh_2O_3 oxide phases were formed, because the latter most likely did not exceed a monolayer [14].

Fig. 8 presents the TOFs of the CO_2 production rate as a function of the oxygen inlet partial pressure. Under open circuit conditions, the TOF of CO_2 formation of the film catalyst was quite low (open circles). The rate of CO_2 formation was positive order with respect to the partial pressure of O_2 under open circuit conditions and became near-zero order under electropromoted conditions. Similarly, the rate was near-zero order

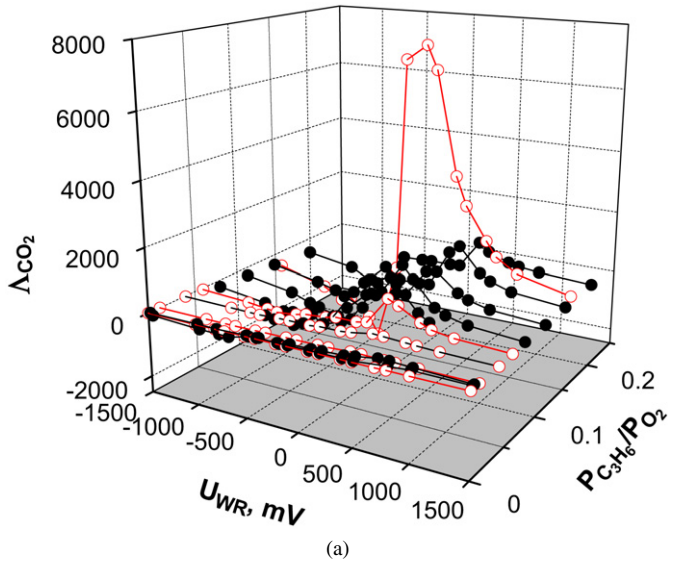

(a)

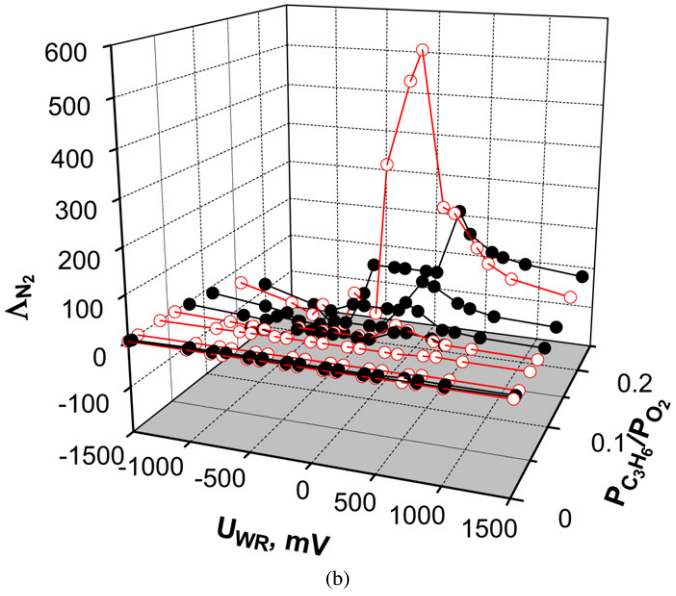

(b)

Fig. 7. Effect of catalyst potential and $P_{C_3H_6}/P_{O_2}$ feed ratio on the Faradaic efficiency of CO_2 formation (a) and N_2 formation (b). Conditions as in Fig. 6.

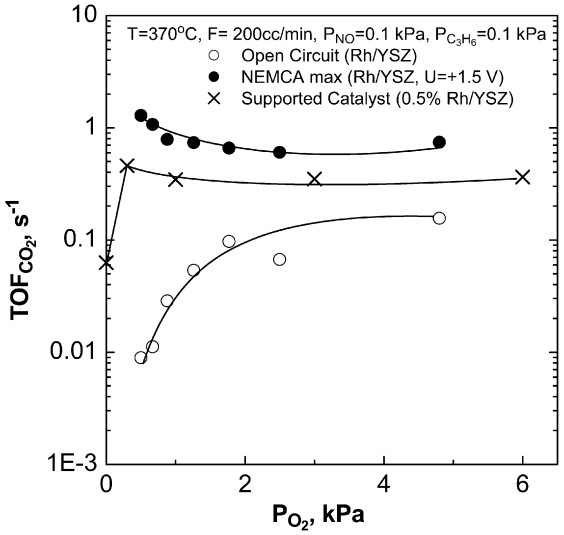

Fig. 8. Effect of P_{O_2} on the TOF of CO_2 formation on the unpromoted (○) and electropromoted (●) Rh film and on the dispersed Rh/YSZ catalyst (×).

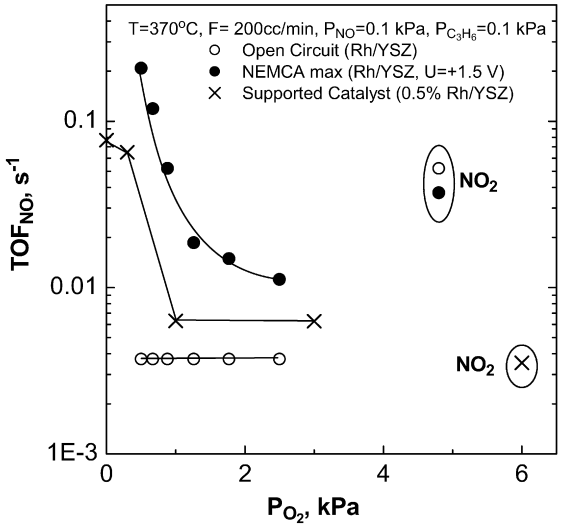

Fig. 9. Effect of P_{O_2} on the TOF of NO conversion to N_2 on the unpromoted (○) and electropromoted (●) Rh film and on the dispersed Rh/YSZ catalyst (×). Encircled points correspond to significant formation of NO_2.

with respect to the oxygen partial pressure for the dispersed catalyst. The TOFs for CO_2 formation of the dispersed catalyst were between the corresponding TOFs for CO_2 of the unpromoted (open circuit) and the electropromoted (closed circuit) catalyst-electrode film.

The TOFs for NO consumption depicted in Fig. 9 show again that the TOF_{NO} of the dispersed Rh/YSZ catalyst was between the corresponding TOFs of the unpromoted and electropromoted Rh paste catalyst-electrodes. The rate of NO consumption was near-zero order with respect to the P_{O_2} for the (highly inactive) unpromoted catalyst and was strongly negative order in P_{O_2} for both the highly active electropromoted Rh paste catalyst-electrode and the dispersed Rh/YSZ catalyst. This is due to the blocking of surface Rh sites by adsorbed O and concomitant formation of surface Rh_2O_3 for values $P_{O_2} > 2.5$ kPa. At $P_{O_2} > 4$ kPa, significant NO_2 formation can be seen for both the electropromoted and the dispersed catalysts.

The results shown in Figs. 8 and 9 underscore the functional similarities and only operational differences between the effect of electrochemical promotion and metal–support interactions with ionic and mixed ionic–electronic conducting supports [14–16].

4. Conclusion

The present study has demonstrated that electrochemical promotion can significantly affect the SCR of NO by propylene, even in the presence of a significant excess of oxygen. The rates of CO_2 and N_2 production are enhanced both with positive (electrophobic behavior) and with negative (electrophilic behavior) potentials or currents. The rate enhancement ratios, ρ,

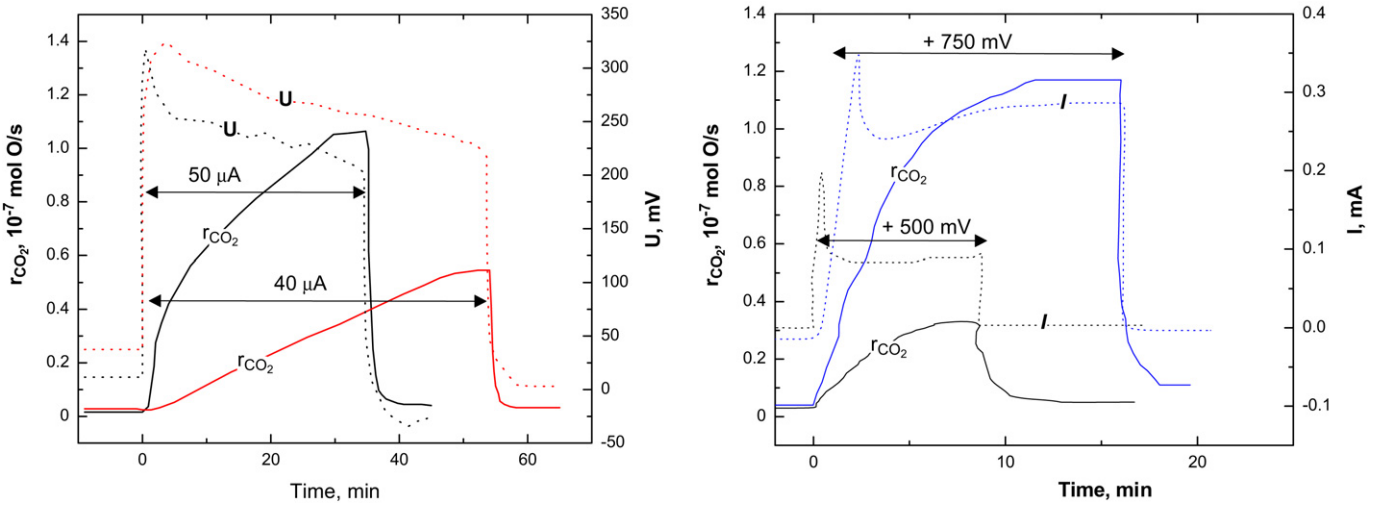

Fig. 10. Galvanostatic (a) and potentiostatic (b) transients used for the measurement of the Rh film surface area, N_G. Conditions for all transients: $P_{NO} = P_{C_3H_6} = 0.1$ kPa, $P_{O_2} = 0.4$ kPa, $T = 370\,^{\circ}C$, $F_v = 200$ cm^3 (STP)/min; galvanostatic transient for 40 μA: $r_0 = 0.02 \times 10^{-7}$ mol O/s, $\Delta r = 0.53 \times 10^{-7}$ mol O/s, $\rho = 27$, $\Lambda = 256$; galvanostatic transient for 50 μA: $r_0 = 0.02 \times 10^{-7}$ mol O/s, $\Delta r = 1.04 \times 10^{-7}$ mol O/s, $\rho = 53$, $\Lambda = 400$; potentiostatic transient for 500 mV: $r_0 = 0.02 \times 10^{-7}$ mol O/s, $\Delta r = 0.3 \times 10^{-7}$ mol O/s, $\rho = 11$, $\Lambda = 58$; potentiostatic transient for 500 mV: $r_0 = 0.05 \times 10^{-7}$ mol O/s, $\Delta r = 1.12 \times 10^{-7}$ mol O/s, $\rho = 23$, $\Lambda = 76$.

for the two main products, CO_2 and N_2, can take very high values. Application of positive current (or potential) leads to ρ values up to 200 and 55 for CO_2 and N_2 production, with apparent Faradaic efficiencies on the order of 7000 and 200, respectively.

Comparing the two phenomena (metal–support interaction with O^{2-}-conducting supports and electrochemical promotion) may lead to the conclusion that they are functionally identical and only operationally different and that the thermal migration (back-spillover) of promoting O^{2-} ions from the support to the metal–gas interface is not sufficient to fully promote a dispersed catalyst (i.e., to establish sufficiently high coverage of O^{2-} on the dispersed catalyst surface), so that the TOFs on the dispersed catalyst do not reach the corresponding TOFs on the fully electropromoted catalyst. This is an important result that shows promise for the practical usefulness of electrochemical promotion.

Similar strong promotional effects are obtained when the support (e.g., Y zeolite) can donate monovalent or divalent cations to the supported metal catalyst [42,43]. This is analogous to the electropromotion of metal films deposited on monovalent or divalent ion-conducting solid electrolytes [3,14,15].

Acknowledgments

The authors thank Toyota for financing this research and Professor Verykios and his laboratory for providing the hydrogen chemisorption measurements on the Rh-dispersed catalyst. D. Archonta and I. Constantinou received graduate student fellowships from the PENED 2001 program of the General Secretariat of Research and Technology (GSRT) Hellas.

Appendix A

Fig. 10 presents two galvanostatic (a) and two potentiostatic (b) transients used to estimate the number of surface Rh mols, N_G, via Eq. (6), that is, $N_G = I\tau/2F$. In the case of the potentiostatic transients, in Eq. (6) we used the time-averaged current value during the rate transient, which differs little (<10%) from the near-steady-state current value obtained after the initial sharp current transients.

As noted earlier, more complex rate versus time transients can be obtained under some conditions (e.g., Fig. 2), apparently due to the abrupt decomposition of the surface monolayer Rh_2O_3 phase [14]. Such transients were not used in computing the average N_G value ($\sim 4 \times 10^{-7}$ mol Rh), but appear to consist of two successive transients each giving a N_G value close to the above average value.

References

[1] C.G. Vayenas, S. Bebelis, S. Ladas, Nature 343 (1990) 625.
[2] R.M. Lambert, F. Williams, A. Palermo, M.S. Tikhov, Top. Catal. 13 (2000) 91.
[3] G. Foti, S. Wodiunig, C. Comninellis, Curr. Top. Electrochem. 7 (2000) 1.
[4] C.A. Cavalca, G.L. Haller, J. Catal. 177 (1998) 389.
[5] L. Ploense, M. Salazar, B. Gurau, E.S. Smotkin, J. Am. Chem. Soc. 119 (1997) 11550.
[6] P. Vernoux, F. Gaillard, L. Bultel, E. Siebert, M. Primet, J. Catal. 208 (2002) 412.
[7] I. Metcalfe, J. Catal. 199 (2001) 247.
[8] C. Sanchez, E. Leiva, in: W. Vielstich, H. Gasteiger, A. Lamm (Eds.), Handbook of Fuel Cells: Fundamentals, Technology and Applications, Wiley, England, 2003.
[9] G. Fóti, O. Lavanchy, Ch. Comninellis, J. Appl. Electrochem. 30 (12) (2000) 1223.
[10] C. Pliangos, C. Raptis, T. Badas, C.G. Vayenas, Ionics 6 (2000) 119–126.
[11] C. Pliangos, C. Raptis, T. Badas, C.G. Vayenas, Solid State Ionics 136/137 (2000) 767–773.
[12] C. Pliangos, C. Raptis, T. Badas, D. Tsiplakides, C.G. Vayenas, Electrochim. Acta 46 (2000) 331–339.
[13] C.G. Vayenas, M.M. Jaksic, S. Bebelis, S.G. Neophytides, in: J.O.M. Bockris, B.E. Conway, R.E. White (Eds.), Modern Aspects of Electrochemistry, Kluwer Academic/Plenum, New York, 1996, p. 57.

[14] C.G. Vayenas, S. Bebelis, C. Pliangos, S. Brosda, D. Tsiplakides, Electrochemical Activation of Catalysis: Promotion, Electrochemical Promotion and Metal–Support Interactions, Kluwer Academic/Plenum, New York, 2001.
[15] C.G. Vayenas, C. Pliangos, S. Brosda, D. Tsiplakides, in: A. Wieckowski, E. Savinova, C.G. Vayenas (Eds.), Catalysis and Electrocatalysis at Nanoparticles, Dekker, New York, 2003.
[16] J. Nicole, D. Tsiplakides, C. Pliangos, X.E. Verykios, Ch. Comninellis, C.G. Vayenas, J. Catal. 204 (2001) 23.
[17] X.E. Verykios, in: A. Wieckowski, E.R. Savinova, C.G. Vayenas (Eds.), Catalysis and Electrocatalysis at Nanoparticles Surfaces, Marcel Dekker, New York, 2003.
[18] S. Bebelis, N. Kotsionopoulos, Solid State Ionics 177 (2006) 2205.
[19] C. Kokkofitis, G. Karagiannakis, S. Zisekas, M. Stoukides, J. Catal. 234 (2) (2005) 476.
[20] M.D. Amiridis, T. Zhang, R.J. Farrauto, Appl. Catal. B 10 (1996) 203.
[21] A. Fritz, V. Pitchon, Appl. Catal. B 13 (1997) 1.
[22] V.I. Parvulescu, P. Grange, B. Delmon, Catal. Today 46 (1998) 233.
[23] T.I. Halkides, D.I. Kondarides, X.E. Verykios, Catal. Today 73 (2002) 213–221.
[24] T. Chafik, D.I. Kondarides, X.E. Verykios, J. Catal. 190 (2000) 446.
[25] T. Chafik, A.M. Efstathiou, X.E. Verykios, J. Phys. Chem. B 101 (1997) 7968.
[26] D.I. Kondarides, T. Chafik, X.E. Verykios, J. Catal. 191 (2000) 147.
[27] C.G. Vayenas, S. Bebelis, I.V. Yentekakis, H.-G. Lintz, Catal. Today 11 (3) (1992) 303.
[28] C.G. Vayenas, I.V. Yentekakis, in: G. Ertl, H. Knötzinger, J. Weitcamp (Eds.), Handbook of Catalysis, VCH, Weinheim, 1997, p. 1310.
[29] C. Cavalca, G. Larsen, C.G. Vayenas, G. Haller, J. Phys. Chem. 97 (1993) 6115.
[30] I.V. Yentekakis, S. Bebelis, J. Catal. 137 (1992) 278.
[31] I. Riess, C.G. Vayenas, Solid State Ionics 159 (3–4) (2003) 313.
[32] D. Tsiplakides, C.G. Vayenas, J. Catal. 185 (1999) 237.
[33] A. Kotsifa, T.I. Halkides, D.I. Kondarides, X.E. Verykios, Catal. Lett. 79 (1–4) (2002) 113.
[34] C. Pliangos, C. Raptis, T. Badas, C.G. Vayenas, Solid State Ionics 136/137 (2000) 767.
[35] C. Raptis, Ph.D. thesis, Department of Chemical Engineering, University of Patras, 2003.
[36] C. Pliangos, Ph.D. thesis, Department of Chemical Engineering, University of Patras, 1995.
[37] C.G. Vayenas, S. Brosda, C. Pliangos, J. Catal. 203 (2001) 329.
[38] C. Pliangos, I.V. Yentekakis, X.E. Verykios, C.G. Vayenas, J. Catal. 154 (1995) 124.
[39] I. Constantinou, Ph.D. thesis, Chemical Engineering Department, University of Patras, 2005.
[40] P. Vernoux, F. Gaillard, R. Karoum, A. Billard, Appl. Catal. B 73 (2007) 73.
[41] F. Dorado, A. de Lucas-Consuegra, P. Vernoux, J.L. Valverde, Appl. Catal. B 73 (2007) 85.
[42] T. Visser, T. Alexander Nijhuis, AdM.J. van der Eerden, K. Jenken, Y. Ji, W. Bras, S. Nikitenko, Y. Ikeda, M. Lepage, B.M. Weckhuysen, J. Phys. Chem. B 109 (2005) 3822.
[43] AdM.J. van der Eerden, T. Visser, T. Alexander Nijhuis, Y. Ikeda, M. Lepage, D.C. Koningsberger, B.M. Weckhuysen, J. Am. Chem. Soc. 127 (2005) 3272.